Available online at www.sciencedirect.com
ScienceDirect
Dyes and Pigments 77 (2008) 635–645
DYES and PIGMENTS
www.elsevier.com/locate/dyepig

Electrochemical studies of bis [1-substituted (−NO_2, −COOH, −Cl, −Br) phenyl-3,5-diphenylformazanato]nickel(II) complexes

Habibe Tezcan*, Elif Uzluk

Department of Chemistry, Gazi University, Faculty of Gazi Education, Teknikokullar, 06500 Ankara, Turkey

Received 18 June 2007; received in revised form 19 September 2007; accepted 25 September 2007
Available online 4 October 2007

Abstract

Bis [1-substituted (−NO_2, −COOH, −Cl, −Br) phenyl-3,5-diphenylformazanato]nickel(II) complexes were synthesized and characterized using elemental analyses, FTIR, GC−mass spectra, ^{1}H NMR, ^{13}C NMR and UV−vis spectra. The electrochemical behavior, number of electrons transferred, diffusion coefficients and heterogeneous rate constants were determined using cyclic voltammetry, ultramicrodisc electrodes and chronoamperometry; possible mechanisms were proposed based on the ensuing data. A correlation between λ_{max} and E_{ox1}, E_{red1} and k_s values was investigated.

Keywords: Nickel complexes of formazans; Spectroscopy; Cyclic voltammetry; Redox properties

1. Introduction

Derivatives of formazans were synthesized and structural features were investigated and the effects of substituents on the absorption λ_{max} values were examined [1−4]. Metal complexes of formazans were synthesized and structural determination, magnetic properties, complex stability constant determination and spectroscopic characterization and the formation of Fe complexes depending upon the pH value were investigated [5−10].

Formazans form tetrazolium salt when they are oxidized [11]. Tetrazolium salts are reduced back to formazans by the enzymes in the cell and stain the tissue. Tetrazolium−formazan system is classified as a marker of vitality and this feature enabled the determination of activity on tumor cell [12,13]. This feature caused an increasing interest in the chemistry and especially electrochemistry of formazans.

The study related to the redox behavior of formazans was carried out and it was claimed that ditetrazolium salts are reduced to both mono and diformazans by one-electron transfers. The first one-electron transfer results in the formation of a tetrazolium radical and this radical was undergoing the disproportion reaction [14].

Formazans are oxidized in a single step two-electron transfer followed by a deprotonation reaction forming corresponding tetrazolium cation [15]. In the reduction of tetrazolium salts into formazans there was one-electron transfer and the electrochemical behavior of nitro formazan derivatives was investigated [16,17].

As seen, many studies have been worked with formazans. But electrochemical studies of their nickel(II) complexes have not been reported in literature. In this study, 13 different nickel(II) complexes of formazans with −NO_2, −COOH, −Cl and −Br substituents in the *o*-, *m*-, *p*-positions of the 1-phenyl ring have been synthesized [4,22] (Scheme 1). Their structures were elucidated by elemental analyses, GC−mass, FTIR, and their spectral behaviors were investigated using ^{1}H NMR, ^{13}C NMR, FTIR and UV−vis spectral data. The effect of substituents on λ_{max} values was determined.

Furthermore in this study we have determined peak potentials (E_{ox}, E_{red}), diffusion coefficients (D), number of electrons transferred (n) and heterogeneous rate constants (k_s) with the

* Corresponding author. Fax: +90 312 2227037.
E-mail address: habibe@gazi.edu.tr (H. Tezcan).

0143-7208/$ - see front matter © 2007 Elsevier Ltd. All rights reserved.
doi:10.1016/j.dyepig.2007.09.009

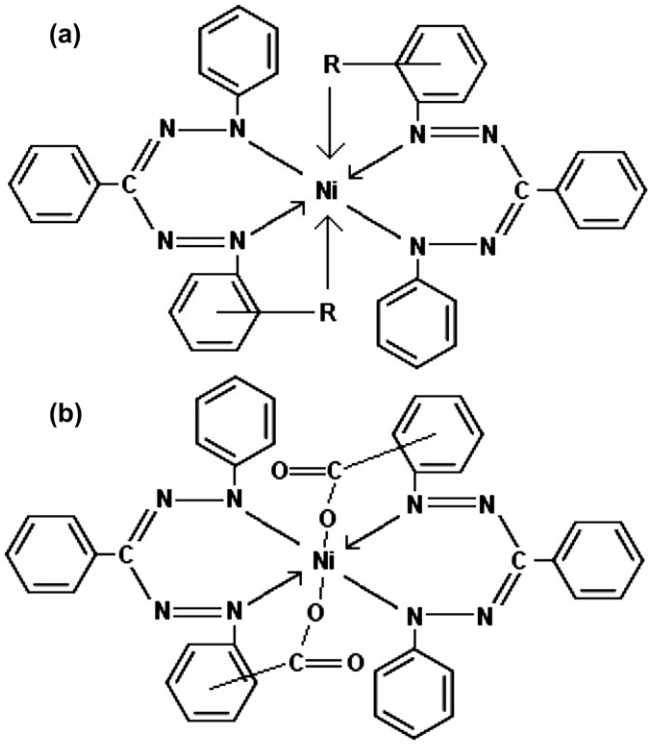

Nickel-Formazan complexes (a, b)	R	Abbreviation
1	H	Ni-TPF
2	*o*-NO_2	Ni-*o*-NPF
3	*m*-NO_2	Ni-*m*-NPF
4	*p*-NO_2	Ni-*p*-NPF
5	-	Ni-*o*-COPF
6	-	Ni-*m*-COPF
7	-	Ni-*p*-COPF
8	*o*-Cl	Ni-*o*-CPF
9	*m*-Cl	Ni-*m*-CPF
10	*p*-Cl	Ni-*p*-CPF
11	*o*-Br	Ni-*o*-BPF
12	*m*-Br	Ni-*m*-BPF
13	*p*-Br	Ni-*p*-BPF

Scheme 1. The structure of the nickel(II) complexes of formazan derivatives (a): **1**–**4** and **8**–**13**; (b): **5**–**7**.

use of cyclic voltammetry, ultramicrodisc electrodes and chronoamperometry. A mechanistic scheme for the oxidation of formazan to tetrazolium salt was proposed based upon these data (Scheme 2).

2. Experimental

2.1. General

All starting reagents and solvents were purchased from Merck, Sigma–Aldrich Chemical Co. and used without further purification. Deionized water (Millipore, Milli-Q) and the organic solvents: CH_3OH (99.9%), CH_3OCH_3 (99.9%) and 1,4-dioxane were used for synthesis, dimethyl sulfoxide (DMSO) (99.9%) was used for spectroscopic measurements and electrochemical measurements.

^{1}H NMR spectra were recorded on a Bruker AVANCE DPX-400 MHz and ^{13}C NMR on a 100 MHz spectrophotometer using $CDCl_3$ and DMSO-d_6, 10^{-4} mol l^{-1}. Elemental analyses were carried out using a LECO-CHNS-932 elemental analyzer and mass spectra were recorded on an AGILENT 1100 MSD LC/MS spectrometer. Absorption spectra were obtained using UNICAM UV2-100 UV–vis spectrophotometer equipped with 1 cm quartz cells in 10^{-5} mol l^{-1} DMSO in the range of 250–700 nm. IR spectra were recorded on a MATT-SON 100-FT-IR spectrophotometer between 4000 and 400 cm^{-1} using KBr pellets.

Electrochemical studies were carried out with a computerized CHI Instrument 660 B system in a conventional three-electrode cell. A platinum electrode (PE) (CHI102), 10 μm-platinum ultramicrodisc electrode (UME) (CHI107) and platinum wire were used. The electrodes were cleaned by electrochemical potential cycling and washed with excess dimethyl sulfoxide. The reference electrode was a silver wire in constant contact with 0.1 M $AgNO_3$ in dimethyl sulfoxide. All solutions were deaerated for 10 min with pure argon and the measurements were taken at room temperature, 25 °C. The supporting electrolyte, tetrabuthylammonium tetrafluoroborate ($TBA^+BF_4^-$) was purchased from Fluka (21796-4). The voltage scan rate range during the CV measuruments was 10–1000 mV/s.

2.2. General synthesis of nickel(II) complexes of formazan

Formazans were synthesized as described in Ref. [4]. Complexes were obtained by the reaction of 1-[*o*-, *m*-, *p*-substituted (–NO_2, –COOH, –Cl, –Br) phenyl]-3,5-diphenylformazans with the metal salt [$Ni(CH_3COO)_2 \cdot 4H_2O$] [22].

2.2.1. Preparation of bis [1-(o-, m-, p-substituted (–NO_2, –COOH, –Cl, –Br) phenyl)-3,5-diphenylformazanato]nickel(II) complexes (**1**–**13**)

Formazans (0.01 mol) obtained as described in Ref. [4] were dissolved in dioxane. In another flask, $Ni(CH_3COO)_2 \cdot 4H_2O$ (0.005 mol) was dissolved in ethanol under reflux with constant stirring at 25 °C to which was added the formazan solution gradually with constant stirring at pH 6–7. The mixtures were stirred at 25–35 °C under reflux for 5–8 h and kept in the dark for 2–3 days. Dyes were filtered and then washed with 10–20 ml 0.5 M NaOH, water and methanol, recrystallized from methanol, dried at 40 °C for 12–24 h.

3. Results and discussion

In this study in the first step, formazans and their nickel(II) complexes were synthesized; in the second step, their structures were elucidated and then spectroscopic properties and the effects of substituents on the absorption properties of

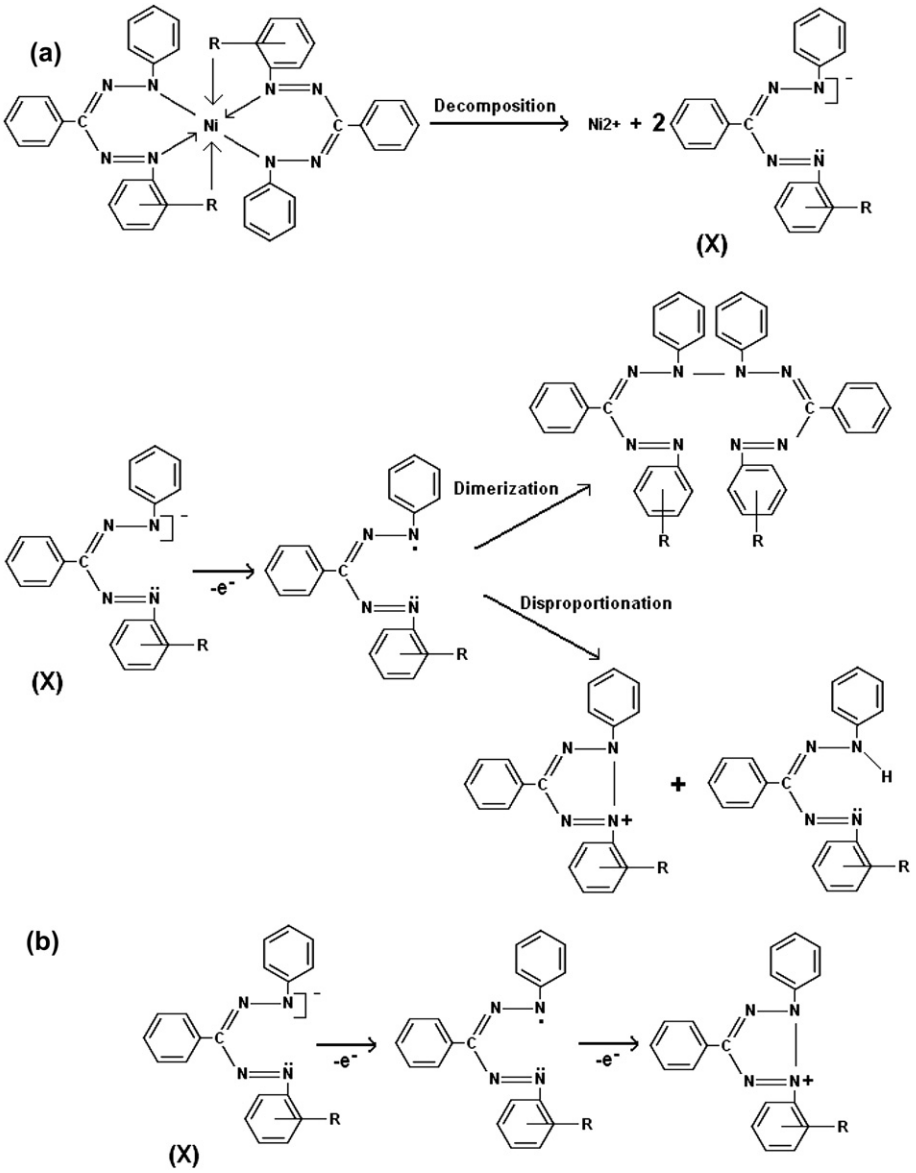

Scheme 2. (a) Possible oxidation mechanism of compound **1** (Ni−TPF), compounds **2**−**4** (Ni−*o*-, *m*-, *p*-NPF) and compounds **6**, **7**, **12**, **13** (Ni−*m*-, *p*-COPF, -BPF). (b) Possible oxidation mechanism of compounds **5**, **11** (Ni−*o*-COPF, -BPF) and compounds **8**−**10** (Ni−*o*-, *m*-, *p*-CPF).

compounds were investigated. In the third step, electrochemical properties were investigated.

The isolated complexes are stable in air, insoluble in water, slightly soluble in anhydrous EtOH, 1,4-dioxane, but soluble in DMSO and DMF. The physical properties, the elemental analysis together with the formula weight obtained from the GC−mass spectra for the complexes are listed in Table 1. The results of the elemental analyses, mass spectra are proved with the proposed structures (Scheme 1).

3.1. Spectral properties

As seen from Table 2 (^{1}H NMR spectral data), aromatic-H peak for Ni−TPF (**1**) observed at $\delta = 8.18-7.45$ ppm were shifted between 8.58 and 6.98 ppm in the substituted nickel(II) complexes. The extent of this shift decreased in the order: $NO_2 > COOH > Br > Cl$, in accordance with the electron withdrawing and donating power of the substituents. The proton of COOH group peaks was observed in the region 12.00−8.00 ppm. The N−H peak observed in the region 2.68−1.18 ppm in formazans disappeared in nickel(II) complexes. This is a further proof that the metal ion was inserted in place of the protons of N−H group and COOH group. These results confirm the proposed formula given in Scheme 1. These data are supported by the IR results.

As seen from Table 2 (^{13}C NMR spectral data), the δ values for the imino-C (C═N) for Ni−TPF (**1**) was observed at 174.81 ppm. δ(C═N) peaks for substituted nickel(II) complexes (**2**−**13**) were observed between 151.23 and 175.50 ppm. But these results showed the effect of changing the type and the position of the substituent on the rings. For instance there was a shift in C═N peak towards higher field when

Table 1
Physical properties, analytical data and formula weight (F.W.) of the prepared nickel(II) complexes

Comp.	Color	M.p. (°C) (lit)	Yield (%) (lit)	Found (Calcd. %)			F.W.	
				C	H	N	Found	Calcd.
1	Light brown	300 (300)	82 (9)	69.90 (69.65)	4.52 (4.58)	17.25 (17.11)	655.00	654.70
2	Light pink-brown	274–275	70	61.14 (61.23)	3.26 (3.49)	18.29 (18.79)	744.10	744.70
3	Yellow-brown	291–292	61	61.17 (61.23)	3.21 (3.49)	18.49 (18.79)	744.30	744.70
4	Violet-black	294–295	50	61.20 (61.23)	3.28 (3.49)	18.18 (18.79)	745.00	744.70
5	Violet	268–269	50	64.07 (64.62)	4.01 (3.77)	14.82 (15.08)	743.50	742.70
6	Yellow	281–282	45	64.11 (64.62)	4.20 (3.77)	15.40 (15.08)	742.90	742.70
7	Brown	298–299	47	64.80 (64.62)	3.85 (3.77)	14.90 (15.08)	742.60	742.70
8a	Light pink-brown	247–248	65	62.75 (63.09)	3.40 (3.59)	15.30 (15.49)	722.50	722.70
9	Light green	276–277	60	63.28 (63.09)	3.23 (3.59)	15.12 (15.49)	722.90	722.70
10a	Light green	289–290	62	63.11 (63.09)	3.47 (3.59)	15.82 (15.49)	723.00	722.70
11	Light pink-brown	264–265	66	55.95 (56.10)	2.95 (3.19)	13.81 (13.78)	812.60	812.70
12	Yellow-green	275–276	65	55.80 (56.10)	2.89 (3.19)	13.20 (13.78)	813.00	812.70
13	Light brown	282–283	40	56.20 (56.10)	3.33 (3.19)	13.64 (13.78)	813.80	812.70

the 1-phenyl ring is substituted with NO_2 (*o*-, *p*-positions), COOH (*o*-, *m*-, *p*-positions) and Br (*m*-, *p*-positions) compared with unsubstituted Ni–TPF (**1**) while there was a shift towards lower fields when 1-phenyl ring is substituted with Cl (*o*-, *m*-, *p*-positions), Br (*o*-position) and NO_2 (*m*-position).

The most characteristic bands of the complexes are summarized in Table 3. As seen from Table 3, ν(C=N) bands at 1589–1446 cm^{-1} and ν(N=N) bands at 1410–1321 cm^{-1} were observed in nickel(II) complexes. These results are in agreement with Refs. [7,21]. The ν(N–H) bands observed in the region 3100–2800 cm^{-1} in formazans disappeared in the nickel(II) complexes. However, new peaks observed at 3089–2937 cm^{-1}, which can be attributed to ligand–metal peaks, have emerged. This is verification of the formation of nickel(II) complexes as a result of insertion of Ni^{2+} in place of an H atom in N–H [6,7,9] and confirmation of the proposed formula given in Scheme 1. The bands observed at 650–450 cm^{-1} were assigned to Ni–N, Ni–O, Ni–Cl and Ni–Br bending vibrations, supporting the ligands such as NO_2, Cl, Br and Ni(II) ion coordination. These results confirm the proposed formula given in Scheme 1. The ν(C=O) stretching bands observed at 1700–1615 cm^{-1} in –COOH group with substituted formazans shifted to lower frequencies (1598–1580 cm^{-1}) in their nickel(II) complexes (**5**–**7**). This can be taken as an evidence for the no participation of COOH groups in chelation [6,9] and confirm the structure given in Scheme 1b. Other aromatic C–H, C=C, CNNC skeleton stretching peaks in the compounds were observed in their expected regions.

As seen from Table 4, the characteristic broad UV–vis peaks observed at 478–489 nm in formazans were observed in the their nickel(II) complexes at 426–446 nm (λ_{max1}). This peak was attributed to the complex formation [4,20]. These results are in agreement with insertion of Ni^{2+} in formazan structure.

3.2. Electrochemical properties

3.2.1. Cyclic voltammetry

The cyclic voltammetric behavior of the nickel(II) complexes of formazans were studied in anhydrous DMSO at room temperature. The cyclic voltammograms of substituted (–NO_2, –COOH, –Cl and –Br) nickel(II) complexes (**2**–**13**) are compared with the parent compound Ni–TPF (**1**). Figs. 1 and 2 show typical cyclic voltammograms of some compounds.

A cyclic voltammogram of Ni–TPF (**1**) is shown in Fig. 1. The scan showed one anodic wave and one cathodic wave. A cyclic sweep in the −1.60 to +0.00 V range shows an anodic peak at $E_{ox1} = -1260.6$ mV and a cathodic peak at $E_{red1} = -798.1$ mV. As seen from Fig. 1, Ni–TPF (**1**) gives one-electron transfer. This complex probably gives dimerization or disproportionation reaction following the radical formation step at −1260.6 mV. However, it seems that the substituted groups (–NO_2,–COOH, –Cl, –Br) have quite an effect upon the electrochemical behavior of the nickel(II) complexes of formazans in Figs. 1 and 2.

As seen from Table 5, the substitution of the 1-phenyl ring with nitro group at the *o*-, *m*-, *p*-positions of compounds **2**–**4** caused major changes in both the peak potential and the peak currents as compared with the parent Ni–TPF (**1**). Compounds **2**–**4** behave similarly towards oxidation; they are oxidized by one-electron processes. These complexes (**2**–**4**) probably give dimerization or disproportionation reaction following the radical formation step.

The scans of complexes **2**–**4** showed one anodic wave and one cathodic wave. On oxidation of –NO_2 substituted nickel(II) complexes, oxidation peaks were observed at more anodic potential in the *o*-, *m*-, *p*-NO_2 complexes **2**–**4** compared with Ni–TPF (**1**). A cyclic sweep in the −1.60 to +0.00 V range shows an anodic peak at $E_{ox1} = -697.6$ mV and a cathodic peak at $E_{red1} = -1303.4$ mV for compound **2**. In the same range, an anodic peak (E_{ox1}) appears at −930.1 mV and a cathodic peak (E_{red1}) is observed at −1004.4 mV for compound **3**. In the same range, an anodic peak (E_{ox1}) is obtained at −1114.2 mV and a cathodic peak (E_{red1}) is observed at −923.3 mV for compound **4**.

As seen from Fig. 1 and Table 5, the substitution of the 1-phenyl ring with carboxyl group at the *o*-, *m*-, *p*-positions (compounds **5**–**7**) caused major changes in both the peak

Table 2
^{1}H NMR and ^{13}C NMR spectral data of the prepared nickel(II) complexes

Comp.	^{1}H NMR[a]	^{13}C NMR[b]	Other explicit carbons
	Aromatic-H, δ (ppm)	Imino-C, (C=N)	
1	8.18–7.45(30H)	174.81	163.97, 161.86, 158.67, 157.90, 155.03, 153.47, 152.20, 150.21, 149.01, 148.61, 142.21, 139.03, 130.42, 127.90, 126.33, 120.59, 118.50 (total 18C)
2	8.58–7.14(28H)	152.80	143.96, 140.76, 137.09, 135.98, 135.00, 133.97, 133.58, 130.52, 129.48, 129.15, 127.21, 126.35, 125.43, 123.24, 122.61, 116.86
3	8.52–7.10(28H)	174.50	160.02, 153.57, 151.07, 150.36, 146.07, 144.28, 142.86, 139.28, 136.07 133.21, 131.78, 129.80, 128.57, 126.07, 124.64, 121.71, 119.64, 116.78
4	8.45–6.98(28H)	175.10	170.46, 167.50, 162.81, 151.72, 147.97, 143.28, 140.62, 135.16, 134.56, 132.35, 129.86, 128.12, 122.50, 112.38
5	8.45–7.36(28H)	175.18	160.04, 157.81, 156.87, 154.37, 153.12, 149.68, 148.12, 145.94, 142.18, 133.75, 130.10, 126.25, 123.75, 122.50, 120.05, 116.87, 115.00, 111.25
6	8.12–7.10(28H)	175.50	160.03, 157.50, 153.33, 151.67, 144.30, 142.64, 139.17, 137.50, 136.53, 135.56, 133.33, 132.64, 130.00, 139.17, 120.00, 117.22, 114.86, 113.34
7	8.28–6.98(28H)	175.10	160.03, 157.06, 150.48, 145.29, 144.90, 144.11, 141.76, 137.35, 133.53, 132.94, 127.35, 124.11, 119.12, 116.76
8a	8.24–7.09(28H)	152.50	150.00, 149.40, 148.47, 147.35, 146.60, 143.85, 142.30, 136.80, 131.00, 130.42, 129.14, 128.75, 127.15, 126.27, 123.50, 121.24, 116.15
9	8.25–7.00(28H)	163.80	154.18, 152.90, 151.51, 147.21, 145.69, 137.28, 136.19, 132.61, 130.54, 130.11, 129.53, 129.28, 127.07, 125.65, 124.37, 124.03, 121.30, 119.78
10a	8.18–6.90(28H)	151.58	150.30, 149.75, 148.72, 147.11, 139.00, 137.50, 128.79, 128.18, 127.09, 125.75, 124.76, 124.36, 122.75
11	8.29–7.05(28H)	151.23	149.53, 147.56, 146.28, 145.11, 143.03, 139.65, 133.72, 133.64, 130.56, 129.37, 129.33, 128.69, 126.81, 126.12, 121.80, 117.04, 114.76
12	8.28–6.98(28H)	175.16	152.00, 151.40, 150.31, 149.37, 148.75, 144.37, 143.75, 141.87, 137.03, 136.25, 135.10, 129.06, 128.59, 125.10, 124.06, 120.47, 120.07, 118.28
13	8.22–7.12(28H)	175.28	154.03, 152.11, 150.38, 148.84, 147.88, 145.96, 144.42, 139.24, 130.12, 125.10, 121.50, 118.23, 116.10, 111.00

[a] The ^{1}H NMR spectra were recorded with 400 MHz (in DMSO-d_6).
[b] ^{13}C NMR spectra were recorded with 100 MHz (in DMSO-d_6).

potential and the peak currents as compared with the parent Ni–TPF (**1**). Compound **5** oxidized in two one-electron processes. Compound **5** forms the formazan radical (TPF$^{\bullet}$) from the formazan anion (TPF^{-}) formed through a one-electron loss which is followed by a one-electron loss to give the corresponding tetrazolium cation (TPT^{+}). Compounds **6** and **7** behave similarly by oxidation; they are oxidized by one-electron processes. These complexes (**6** and **7**) probably give dimerization or disproportionation reaction following the radical formation step. On oxidation of COOH nickel(II) complexes, oxidation peak was observed at a more cathodic potential in the *o*-, *p*-COOH complexes **5** and **7** and at a more anodic potential in the *m*-COOH complex **6** compared to Ni–TPF (**1**).

The scan of compound **5** showed two anodic waves and one cathodic wave. A cyclic sweep in the −1.60 to +0.00 V range shows two anodic peaks at $E_{ox1} = -1425.3$ mV, $E_{ox2} = -891.9$ mV and a cathodic peak at $E_{red1} = -926.1$ mV for compound **5** (Fig. 1). The scans of compounds **6** and **7** showed one anodic wave and one cathodic wave. In the −1.60 to +0.00 V range, an anodic peak (E_{ox1}) appears at −1205.8 mV and a cathodic peak (E_{red1}) is observed at −727.3 mV for compound **6** (Fig. 1). In the same range, an anodic peak (E_{ox1}) is obtained at −1462.0 mV and a cathodic peak (E_{red1}) is observed at −726.0 mV for compound **7** (Fig. 1).

The $-NO_2$ group at a more anodic potential was shifted with reference to −COOH group when substitutents were compared with each other. This result is in agreement with the fact that $-NO_2$ group is a stronger electron withdrawing group as compared to −COOH group.

As seen from Table 5, the substitution of the 1-phenyl ring with chloro at the *o*-, *m*-, *p*-positions of compounds **8–10** caused major changes in both the peak potential and the peak currents as compared with the parent Ni–TPF (**1**). Compounds **8–10** behave similarly towards oxidation; they are oxidized in two one-electron processes. Compounds **8–10** form the formazan radical (TPF$^{\bullet}$) from the formazan anion (TPF^{-}) formed through a one-electron loss which is followed by a one-electron loss to give the corresponding tetrazolium cation (TPT^{+}).

At the oxidation of Cl nickel(II) complexes, oxidation peak was observed at a more cathodic potential in the *o*-, *p*-Cl complexes **8** and **10** and at a more anodic potential in the *m*-Cl complex **9** compared with Ni–TPF (**1**).

The scans of compounds **8–10** showed two anodic waves and one cathodic wave. A cyclic sweep in the −1.60 to +0.00 V range shows two anodic peaks at $E_{ox1} = -1490.8$ mV, $E_{ox2} = -988.8$ mV, respectively, and a cathodic peak at $E_{red1} = -884.3$ mV for compound **8**. In the same range, two anodic peaks appear at $E_{ox1} = -1218.8$ mV, $E_{ox2} = -481.5$ mV, respectively, and a cathodic peak at $E_{red1} = -756.1$ mV for compound **9**. In the same range, two anodic peaks are obtained at $E_{ox1} = -1537.7$ mV, $E_{ox2} = -939.1$ mV, respectively, and a cathodic peak at $E_{red1} = -894.7$ mV for compound **10**.

As seen from Fig. 2 and Table 5, the substitution of the 1-phenyl ring with bromo at the *o*-, *m*-, *p*-positions compounds **11–13** caused major changes in both the peak potential and

Table 3
The IR spectral data of nickel(II) complexes (**1**–**13**) (KBr, cm^{-1})

Comp.	Aromatic, C–H	Aromatic, C=C	C=N	N=N	C=O	–C–O–Ni	N–Ni	CNNC struc. vibr.
1	3098–3025	1600	1500	1410	–	–	3089	780–550
2	3071–3048	1660	1589	1357	–	–	3030	750–598
3	3070–3040	1660	1580	1357	–	–	2981	750–600
4	3070–3035	1630	1570	1357	–	–	3000	725–620
5	3063–3018	1660	1527	1375	1589	3410–3375	2985	750–652
6	3070–2975	1678	1553	1392	1598	3410–3375	2940	750–642
7	3120–3052	–	1526	1365	1580	3402–3375	2995	750–598
8	3027–3000	1630	1571	1339	–	–	2937	750–598
9	3053–2998	1651	1580	1348	–	–	2971	760–643
10	3053–3000	1598	1495	1378	–	–	2937	803–625
11	3035	1607	1498	1321	–	–	2981	767–630
12	3053–3017	1553	1446	1380	–	–	2937	755–625
13	3027–2973	1589	1446	1339	–	–	2971	750–678

the peak currents as compared to the parent Ni–TPF (**1**). Compound **11** oxidized in two one-electron processes. Compound **11** forms the formazan radical ($TPF^{\bullet}$) from the formazan anion (TPF^{-}) formed through a one-electron loss which is followed by a one-electron loss to give the corresponding tetrazolium cation (TPT^{+}). Compounds **12** and **13** behave similarly towards oxidation; they are oxidized through one-electron processes. These complexes (**12** and **13**) probably give dimerization or disproportionation reaction following the radical formation step. On oxidation of Br nickel(II) complexes, oxidation peak was observed at a more cathodic potential in the *o*-, *p*-Br complexes **11** and **13** and at a more anodic potential in the *m*-Br complexes **12** compared to Ni–TPF (**1**).

The scan of compound **11** showed two anodic waves and one cathodic wave. A cyclic sweep in the −1.60 to +0.00 V range shows two anodic peaks at $E_{ox1} = -1563.9$ mV, $E_{ox2} = -941.7$ mV and a cathodic peak at $E_{red1} = -868.5$ mV for compound **11** (Fig. 2). The scans of compounds **12** and **13** showed one anodic wave and one cathodic wave. In the −1.60 to +0.00 V range, an anodic peak (E_{ox1}) appears at −1177.0 mV and a cathodic peak (E_{red1}) is observed at −719.6 mV for compound **12** (Fig. 2). In the same range, an anodic peak (E_{ox1}) is obtained at −1396.7 mV and a cathodic peak (E_{red1}) is observed at 902.4 mV for compound **13** (Fig. 2).

Table 4
Absorption spectral data for nickel(II) complexes **1**–**13** (in DMSO, 10^{-5} mol/l)

Comp.	λ_{max1} (nm)	Chemical shift $\Delta\lambda_{max}$
1	442.0 (0.283)	–
2	429.0 (0.640)	13
3	440.0 (0.383)	2
4	444.0 (0.548)	−2
5	431.0 (0.347)	9
6	426.0 (0.265)	16
7	446.0 (0.356)	−4
8	435.0 (0.708)	7
9	435.0 (0.355)	7
10	438.0 (0.375)	4
11	436.0 (0.286)	6
12	436.0 (0.208)	6
13	437.0 (0.678)	5

Column 3: $\Delta\lambda_{max} = \lambda_{max1}$ (Ni–TPF) − λ_{max1} (nickel(II)-substituted formazans).

The E_{ox1} values of compounds **8** and **10** are shifted towards more cathodic values compared to Ni–TPF (**1**). At *o*-position –Cl (**8**) is inductively electron withdrawing and electron donating as a result of resonance. Since these effects oppose each other *o*-position has the least electron donating effect to the system and the potential value observed verifies this fact. At *p*-position –Cl (**10**) the inductive effect completely diminishes and resonance effect predominates. That is why E_{ox1} values give the highest cathodic shift at this position. Similar arguments are valid for Br substitution (comps. **11** and **13**). The difference may stem from the difference in electronegativity values. Consequently, peak potentials are dependent upon the type and position of substituents.

3.3. Ultramicrodisc electrode and chronoamperometry

The number of electrons transferred (n) and the diffusion coefficients (D) were determined by the ultramicroelectrode CV technique of Baranski [18]. The diffusion coefficients (D) of the compounds **1**–**13** were calculated from the Cottrell

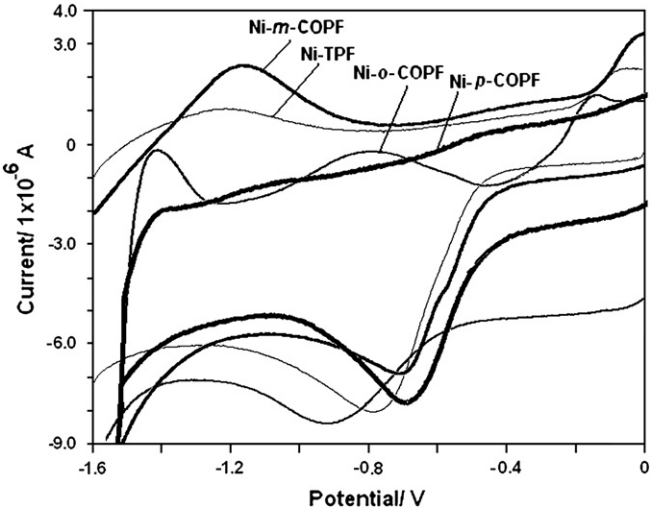

Fig. 1. Representative cyclic voltammogram in DMSO (25 °C, ionic strength: 0.1 M $TBA^{+}BF_4^{-}$, v: 100 mV s^{-1}): compounds Ni–TPF (**1**), Ni–*o*-COPF (**5**), Ni–*m*-COPF (**6**), Ni–*p*-COPF (**7**).

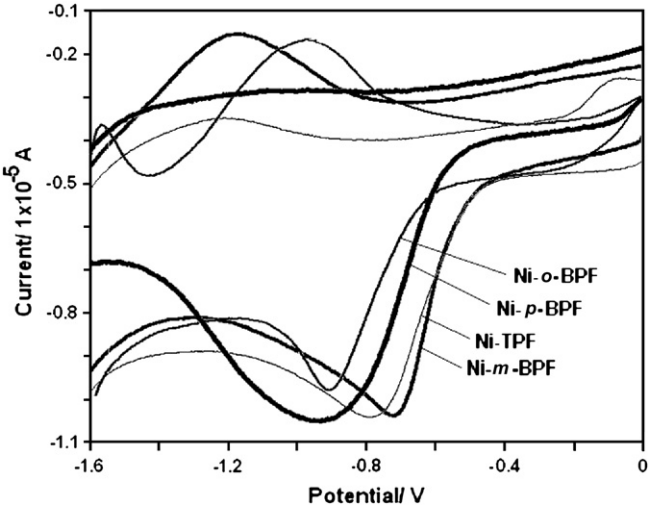

Fig. 2. Representative cyclic voltammogram in DMSO (25 °C, ionic strength: 0.1 M $TBA^+BF_4^-$, v: 100 mV s^{-1}): compounds Ni−TPF (**1**), Ni−*o*-BPF (**11**), Ni−*m*-BPF (**12**), Ni−*p*-BPF (**13**).

equation after the n values had been obtained. The D values are tabulated in Table 6. The heterogeneous rate constants were calculated according to the Klingler−Kochi method [19]. The k_s values were determined with the use of Klinger−Kochi equation as the potential difference for the anodic and cathodic peak currents for the second peak was more than 70 mV. The k_s values under these circumstances are dependent on the scan rate, diffusion coefficient, oxidation and reduction peak potential values.

The oxidation of the nickel(II) complex of formazan derivatives was found to be quasi-reversible due to the fact that ΔE_p is larger than $59/n$ (mV), which increased with the scan rate, and the shift of the anodic peak potential E_{ox} towards positive values with increasing scan rate. The case $2 \times 10^{-5} v^{1/2} < k_s < 0.3v^{1/2}$ corresponds to a quasi-reversible situation. The k_s values obtained in this study fall in this range. The change of the k_s values are in the order: $o- > m- > p$-substitutions for $-NO_2$ substituted nickel(II) complexes of formazans, $p- > m- > o$-substitutions for −COOH substituted nickel(II) complexes of formazans, $m- > p- > o$-substitutions for −Cl substituted nickel(II) complexes of formazans, $p- > o- > m$-substitutions for −Br substituted nickel(II) complexes of formazans (Table 5). The k_s value of unsubstituted nickel(II) complex (Ni−TPF) and p-Br substituted nickel(II) complex are comparatively larger than the others. These results are in agreement with their diffusion coeffcients which are comparatively larger than the others.

Table 5
Voltamperometric results of nickel(II) complexes (**1**–**13**)

Comp.	E_{ox1} (mV)	E_{ox2} (mV)	E_{red1} (mV)	ΔE_p (mV)	k_s (cm s^{-1})
1	−1260.6	–	−798.1	−462.5	11.964×10^{-3}
2	−697.6	–	−1303.4	−605.8	3.946×10^{-3}
3	−930.1	–	−1004.4	−74.3	1.516×10^{-3}
4	−1114.2	–	−923.3	−190.9	1.057×10^{-3}
5	−1425.3	−891.9	−926.1	−499.2	5.613×10^{-3}
6	−1205.8	–	−727.3	−478.0	2.485×10^{-3}
7	−1462.0	–	−726.0	−736.0	9.374×10^{-3}
8	−1490.8	−988.8	−884.3	−606.5	3.682×10^{-3}
9	−1218.8	−481.5	−756.1	−462.7	4.375×10^{-3}
10	−1537.7	−939.1	−894.7	−643.0	3.814×10^{-3}
11	−1563.9	−941.7	−868.5	−695.4	3.587×10^{-3}
12	−1177.0	–	−719.6	−457.4	3.579×10^{-3}
13	−1396.7	–	−902.4	−494.3	15.905×10^{-3}

Column 5: ΔE_p: $E_{ox1} - E_{red1}$ (mV). Cyclic voltammograms were obtained in DMSO at 25 °C at platinum electrode, ionic strength 0.1 M (TBATFB), sweep speed: 100 mV s^{-1}. E_{ox}: oxidation; E_{red}: reduction, k_s (cm s^{-1}) values.

3.3.1. The relation between the E_{ox1} and E_{red1}/mV (Ag/AgCl) and k_s (cm s^{-1}) values

There was a correlation between the peak potentials (E_{ox1} and E_{red1} values) and k_s (cm s^{-1}) (Figs. 3 and 4). This result is in agreement with the fact that k_s values are dependent on the oxidation and reduction peak potential values.

3.3.2. The calculation of the number of electrons transferred

The number of electrons transferred was obtained with the use of chronoamperometric Cottrell equation and ultramicro Pt disc electrode (UME) steady state current (I_{ss}) [18].

The real surface area of the Pt electrode was found to be 2.58 cm^2 with the use ferrocene. If i_t values are plotted against $t^{-1/2}$ from the resulting slope n could easily be calculated. The number of electrons calculated are given in Table 6.

The number of electrons transferred was obtained with the use of chronoamperometry Cottrell equation (Eq. (1))

$$i_t = \frac{nFACD^{1/2}}{\pi^{1/2} t^{1/2}} \tag{1}$$

and ultramicrodisc electrode (UME) steady state current (I_{ss}) (Eq. (2)) [19].

$$i_{ss} = 4rnFCD \tag{2}$$

The real surface area of the Pt electrode was found to be 2.58 cm^2 with the use of ferrocene. If i_t values are plotted against $t^{-1/2}$ from the resulting slope (Eq. (3)) n could easily be calculated.

$$\text{Slope} = \left(\frac{nFC}{\pi r}\right)^{1/2} A \tag{3}$$

The n values calculated are tabulated in Table 6. The number of electrons transferred was found to be in accordance with the CV data (Table 5). The diffusion coefficients were also found within expected dimensions. The results of UME and chronoamperometric data are tabulated in Table 6.

As seen from Fig. 5 and Table 6, there is a one-electron transfer wave for Ni−TPF (**1**). Ni−TPF (**1**) is fragmented. Ni^{2+} and TPF^- anion (X) are formed in solution (Scheme 2). TPF^- anion gives a single one-electron transfer giving a formazan radical ($TPF^{\bullet}$). These radicals give a disproportionation reaction to give a formazan (TPF) and tetrazolium cation (TPT^+) or a dimerization reaction resulting in a diformazan.

Table 6
Some of the parameters calculated for nickel(II) complexes (**1**–**13**)

Comp.	Abbreviation	C^* (mM)	$\dot{I}_{ss}$ (A)	Cottrell slope ($S \times 10^{-5}$)	n	n net	D ($cm^2\,s^{-1}$)
1	Ni–TPF	7.8	4.417×10^{-10}	1.249	0.88	1	1.667×10^{-6}
2	Ni–*o*-NPF	8.8	8.556×10^{-11}	0.610	0.96	1	2.518×10^{-7}
3	Ni–*m*-NPF	7.3	2.027×10^{-11}	0.276	0.87	1	0.719×10^{-7}
4	Ni–*p*-NPF	7.0	6.678×10^{-12}	0.137	0.78	1	0.247×10^{-7}
5	Ni–*o*-COPF	7.6	1.617×10^{-10}	1.076	1.83	2	2.756×10^{-7}
6	Ni–*m*-COPF	8.4	1.493×10^{-10}	0.245	0.93	1	4.604×10^{-7}
7	Ni–*p*-COPF	7.4	2.529×10^{-9}	0.827	0.71	1	8.855×10^{-7}
8	Ni–*o*-CPF	8.1	7.977×10^{-11}	0.881	1.75	2	1.275×10^{-7}
9	Ni–*m*-CPF	8.0	3.527×10^{-11}	0.494	1.68	2	0.572×10^{-7}
10	Ni–*p*-CPF	8.5	1.116×10^{-10}	0.895	1.64	2	1.701×10^{-7}
11	Ni–*o*-BPF	7.1	8.431×10^{-10}	2.282	1.69	2	1.538×10^{-6}
12	Ni–*m*-BPF	7.0	5.173×10^{-11}	0.405	0.88	1	1.914×10^{-7}
13	Ni–*p*-BPF	8.1	0.477×10^{-9}	0.136	0.93	1	1.525×10^{-6}

Mechanism of the oxidation of compound **1** is shown in Scheme 2a. These results are in agreement with Refs. [14,17].

As seen from Table 6, there are one-electron transfer waves for compounds **2**–**4**. The number of electrons transferred are one for *o*-, *m*-, *p*-NO_2 substituted nickel(II) complexes in UME based cyclic voltammograms and chronoamperometry. This is in accordance with CV results. The appearance of one distinctive peak in *o*-, *m*-, *p*-NO_2 substituted nickel(II) complexes suggests that the compounds give one-electron transfer. These complexes (**2**–**4**) are fragmented. Ni^{2+} and substituted formazan radicals are formed in solution (Scheme 2). These radicals give a disproportionation reaction to give a substituted formazan and tetrazolium cation or a dimerization reaction resulting in a diformazan. Mechanism of the oxidation of *o*-, *m*-, *p*-NO_2 substituted nickel(II) complexes (**2**–**4**) are shown in Scheme 2a. These results are in agreement with Refs. [14,17].

As seen from Fig. 5, there are one-electron transfer waves for compounds **6** and **7**. The number of electrons transferred are one for *m*-, *p*-COOH substituted nickel(II) complexes in UME based cyclic voltammograms and chronoamperometry (Table 6). This is in accordance with CV results (Fig. 1). The appearance of one distinctive peak in *m*-, *p*-COOH substituted nickel(II) complexes suggest that the compounds give one-electron transfer. These complexes (**6** and **7**) are fragmented. Ni^{2+} and substituted formazan radicals are formed in solution (Scheme 2). These radicals undergo a disproportionation reaction to give a substituted formazan and tetrazolium cation or a dimerization reaction resulting in a diformazan. Mechanism of the oxidation of *m*-, *p*-COOH substituted nickel(II) complexes (**6** and **7**) is shown in Scheme 2a. These results are in agreement with Refs. [14,17].

As seen from Fig. 6, there are one-electron transfer waves for compounds **12** and **13**. The number of electrons transferred are one for *m*-, *p*-Br substituted nickel(II) complexes in UME based cyclic voltammograms and chronoamperometry (Table 6). This is in accordance with CV results (Fig. 2). The appearance of one distinctive peak in *m*-, *p*-Br substituted nickel(II) complexes suggest that the compounds give one-electron transfer. These complexes (**12** and **13**) are fragmented. Ni^{2+} and substituted formazan radicals are formed in solution

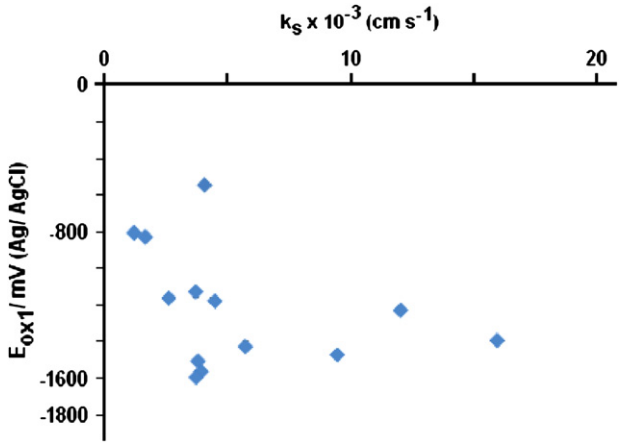

Fig. 3. The correlation between the E_{ox1}/mV (Ag/AgCl) and k_s ($cm\,s^{-1}$) values.

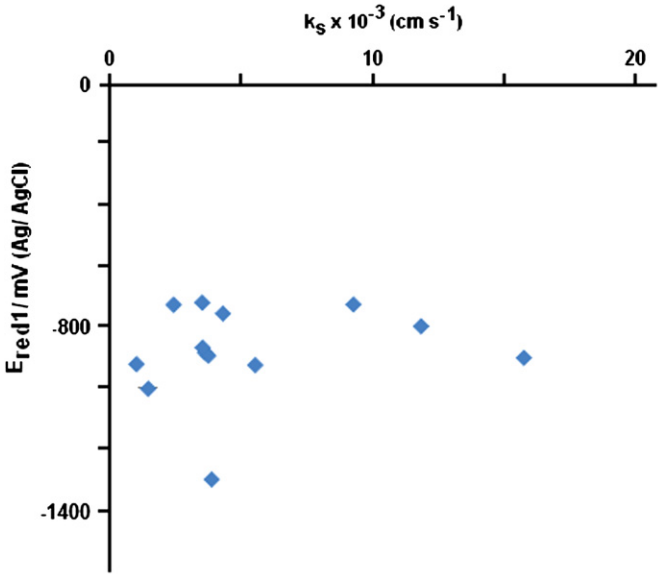

Fig. 4. The correlation between the E_{red1}/mV (Ag/AgCl) and k_s ($cm\,s^{-1}$) values.

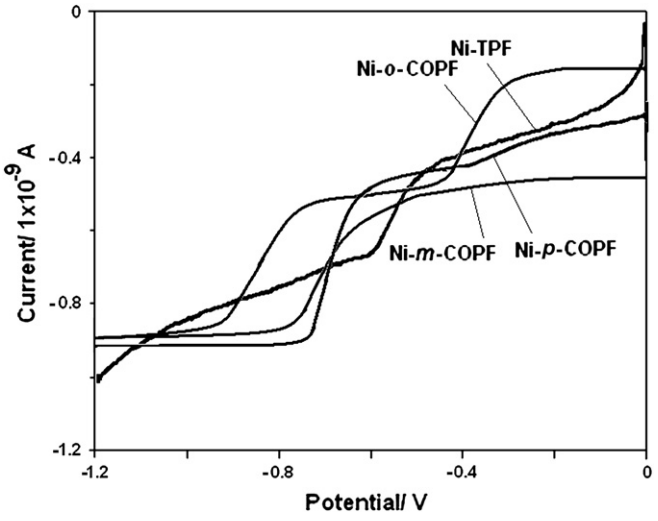

Fig. 5. UME curves of DMSO solutions of 1.0×10^{-5} M compounds Ni–TPF (**1**), Ni–*o*-COPF (**5**), Ni–*m*-COPF (**6**) and Ni–*p*-COPF (**7**) in the presence of 0.1 M $TBA^+BF_4^-$ at 10 μm-platinum ultramicroelectrode. Potential scan rate: 10 mV s^{-1}.

(Scheme 2). These radicals give a disproportionation reaction to give a substituted formazan and tetrazolium cation or a dimerization reaction resulting in a diformazan. Mechanism of the oxidation of *m*-, *p*-Br substituted nickel(II) complexes (**12** and **13**) is shown in Scheme 2a. These results are in agreement with Refs. [14,17].

The nickel(II) complex of *o*-COOH (**5**) substituted gave clear S shaped steady state current (I_{ss}) with UME (Fig. 6). As seen from Fig. 6, there are two one-electron transfer waves for compound **5**. The number of electrons transferred is two for *o*-COOH substituted nickel(II) complex in UME based cyclic voltammogram and chronoamperometry (Table 6). This is in accordance with CV results (Fig. 1). The appearance of two distinctive peaks in *o*-COOH substituted nickel(II) complex

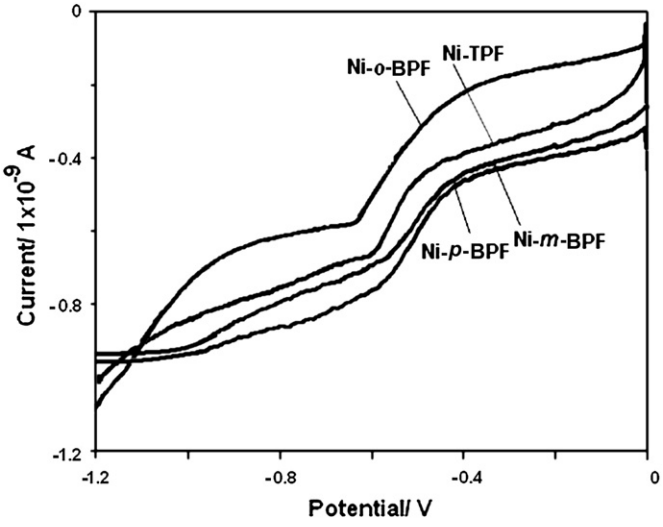

Fig. 6. UME curves of DMSO solutions of 1.0×10^{-5} M compounds Ni–TPF (**1**), Ni–*o*-BPF (**11**), Ni–*m*-BPF (**12**) and Ni–*p*-BPF (**13**) in the presence of 0.1 M $TBA^+BF_4^-$ at 10 μm-platinum ultramicroelectrode. Potential scan rate: 10 mV s^{-1}.

Table 7
The σ and related λ_{max} values

Substituent position	Comp.	Abbreviation	σ' values	λ_{max1} (nm)
	1	H	H: 0	442.0
m-	**3**	*m*-NO_2	*m*-NO_2: 0.71	440.0
	6	*m*-COOH	*m*-COOH: 0.35	426.0
	9	*m*-Cl	*m*-Cl: 0.37	435.0
	12	*m*-Br	*m*-Br: 0.37	436.0
p-	**4**	*p*-NO_2	*p*-NO_2: 0.81	444.0
	7	*p*-COOH	*p*-COOH: 0.44	446.0
	10	*p*-Cl	*p*-Cl: 0.24	438.0
	13	*p*-Br	*p*-Br: 0.26	437.0

suggests that the compound gives two-electron transfers. This complex (**5**) is fragmented. Ni^{2+} and substituted formazan radical are formed in solution (Scheme 2). Compound **5** forms the substituted formazan radical from the substituted formazan anion through a one-electron loss which is followed by a one-electron loss to give the corresponding tetrazolium cation. The two-electron oxidation product (substituted tetrazolium tetrafluoroborate) is formed through oxidation of the parent substituted formazan to a radical (substituted formazan radical) and then cyclised. Mechanism of the oxidation of *o*-COOH substituted nickel(II) complex (**5**) is shown in Scheme 2b. This result is in agreement with Ref. [16].

The nickel(II) complexes of *o*-Cl (**8**) and *m*-Cl (**9**) substituted formazans gave clear S shaped steady state currents (I_{ss}) with UME. As seen from Table 6, there are two one-electron transfer waves for compounds **8**–**10**. The number of electron transferred is two for *o*-, *m*-, *p*-Cl substituted nickel(II) complexes in UME based cyclic voltammogram and chronoamperometry. This is in accordance with CV results. The appearance of two distinctive peaks in *o*-, *m*-, *p*-Cl substituted nickel(II) complexes suggest that the compounds give two-electron transfers. These complexes (**8**–**10**) are fragmented. Ni^{2+} and substituted formazan radicals are formed in solutions (Scheme 2). Compounds **8**–**10** form the substituted formazan radical from the substituted formazan anion through a one-electron loss which is followed by a one-electron loss to give the corresponding tetrazolium cation. Mechanism of the oxidation of *o*-, *m*-, *p*-Cl substituted nickel(II) complexes

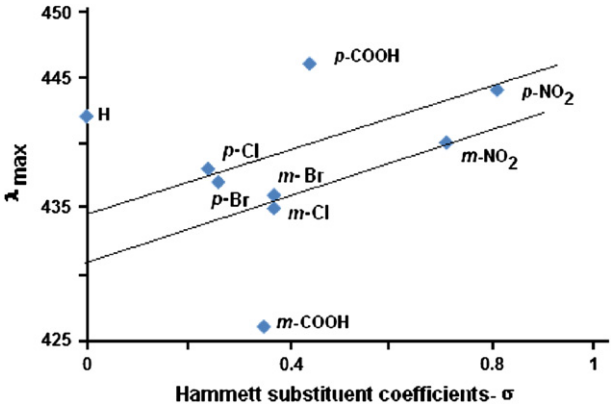

Fig. 7. The λ_{max} values against Hammett substituent coefficients – σ.

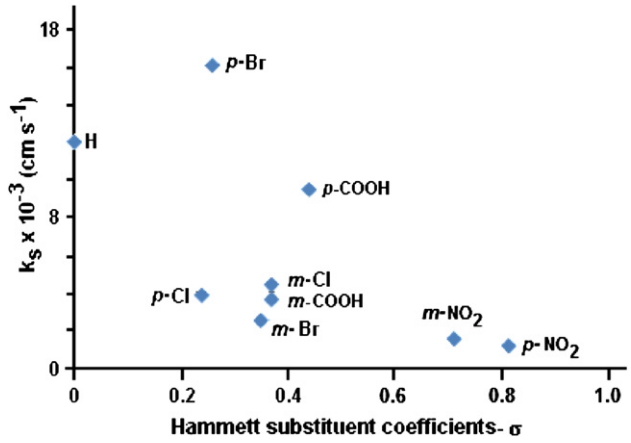

Fig. 8. The k_s values against Hammett substituent coefficients − σ.

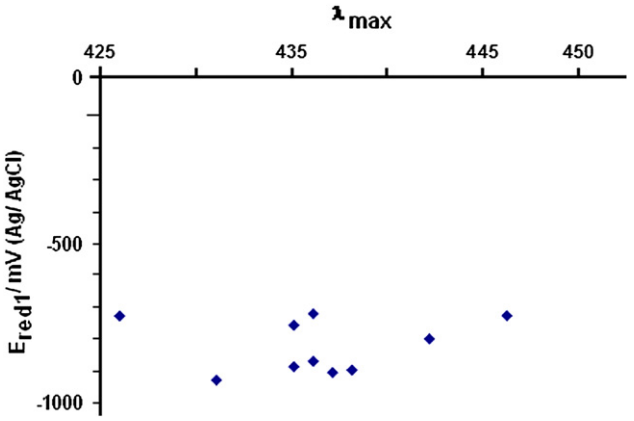

Fig. 10. The correlation between the λ_{max} and the E_{red1}/mV (Ag/AgCl) values.

(**8**–**10**) is shown in Scheme 2b. This result is in agreement with Ref. [16].

As seen from Fig. 6, there are two one-electron transfer waves for compound **11**. The number of electrons transferred is two for *o*-Br substituted nickel(II) complex in UME based cyclic voltammogram and chronoamperometry (Table 6). This is in accordance with CV results (Fig. 2). The appearance of two distinctive peaks in *o*-Br substituted nickel(II) complex suggests that the compound gives two-electron transfers. This complex (**11**) is fragmented. Ni^{2+} and substituted formazan anion are formed in solution (Scheme 2). Compound **11** forms the substituted formazan radical from the substituted formazan anion through a one-electron loss which is followed by a one-electron loss to give the corresponding tetrazolium cation. Mechanism of the oxidation of *o*-Br substituted nickel(II) complex (**11**) is shown in Scheme 2b. This result is in agreement with Ref. [16].

4. Conclusions

Nickel(II) complexes of formazans were prepared and characterized based on their absorption and redox behavior.

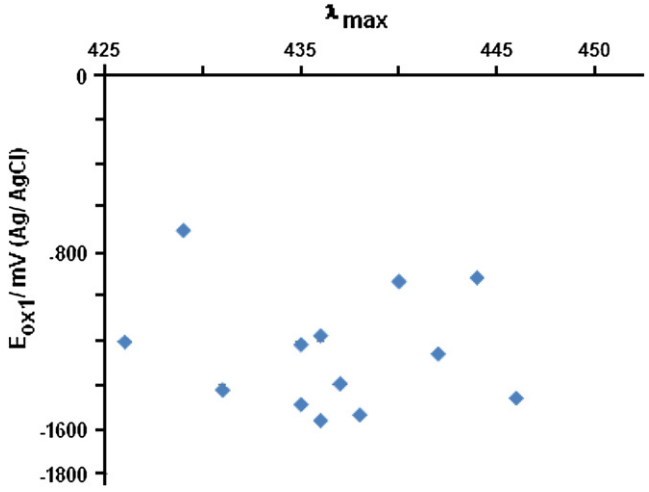

Fig. 9. The correlation between the λ_{max} and the E_{ox1}/mV (Ag/AgCl) values.

Additional support to the above proposed electro-oxidation scheme was found to be of importance. Thus, it appeared mandatory to study the effect of substituent on the reaction site of these compounds. The relationship between Hammett subsituent coefficients (σ) and λ_{max} are tabulated in Table 7. The λ_{max} values have been correlated to Hammett substituent coefficients (σ). The representative λ_{max}–σ plots are illustrated in Fig. 7. As seen from Fig. 7, there was a linear correlation between *m*-position's Hammett substituent coefficient (σ_m) and λ_{max} and a linear correlation between *p*-position's Hammett substituent coefficient (σ_p) and λ_{max}.

Also there was a correlation between σ and k_s (cm^{-1}) (Fig. 8). The spectral and redox properties were compared. There was a correlation between the λ_{max} and peak potentials (E_{ox1} and E_{red1} values) (Figs. 9 and 10).

As seen from Table 5, E_{ox1} values observed at −1260.6 mV in the Ni–TPF (**1**) were shifted to −697.6 to −1537.7 mV in the substituted nickel(II) complexes of formazans (**2**–**13**). The extent of this shift decreased in the order: $NO_2 > COOH > Br > Cl$, in accordance with the electron withdrawing and donating power of the substituents. Since NO_2 and COOH groups are electron withdrawing with regard to both resonance and inductive effects. Their effect on the shift of E_{ox1} to the anodic region are relatively large. Since NO_2 group is a stronger electron withdrawing group than COOH group, its shifting power is much higher. The Cl and Br groups are electron withdrawing with regard to inductive effect but electron donating with regard to resonance and their effect upon the system is the summation of these two opposite effects. That is why their effect to shift E_{ox1} to anodic region is much lower than those of NO_2 and COOH. The findings are as expected. But these results showed the effect of changing the type and the position of the substituent on the rings.

References

[1] Lewis JW, Sandorfy C. Can J Chem 1983;61:809–16.
[2] Katritzky AR, Belyakov SA, Cheng D, Durst HD. Synthesis 1995;5:577–81.

[3] Tezcan H, Sendil Can, Tezcan R. Dyes Pigments 2002;52:121–7.
[4] Tezcan H, Uyar T. Turkish J Spectrosc Aegean Univ 1988;9:8–19.
[5] Gok Y, Tufekci M, Ozcan E. Synth React Inorg Met Org Chem 1993;23:861–73.
[6] Issa YM, Rizk MS, Tayor WS, Soliman MH. J Indian Chem Soc 1993;70:5–7.
[7] Brown DA, Bögge H, Lipunova GN, Müller A, Plass W, Walsh KG. Inorg Chim Acta 1998;280:30–8.
[8] Uchiumi A, Takatsu A, Tanaka H. Anal Sci 1991;7:459–62.
[9] Sherif OE, Issa YM, Hassouna MEM, Abass SM. Monatsh Chem 1993;124:627–35.
[10] Czajkowski W, Stolarski R, Szymczyk M, Wrzeszcz G. Dyes Pigments 2000;47:143.
[11] Schiele VC. Ber 1964;30:308–18.
[12] Mattson AM, Jensen CO, Dutcher RA. Science 1947;5:294–5.
[13] Wan H, Williams R, Doherty P, Williams DF. J Mater Sci Mater Med 1994;5:154–9.
[14] Umemoto K. Bull Chem Soc Jpn 1989;62:3783–9.
[15] Abou Elenien GM. J Electroanal Chem 1994;375:301–5.
[16] Oritani T, Fukuhara N, Okajima T, Kitamura F, Ohsaka T. Inorg Chim Acta 2004;357:436–42.
[17] Gökce G, Durmus Z, Tezcan H, Kılıc E, Yılmaz H. Anal Sci 2005;21:1–4.
[18] Baranski AS, Fawcett WR, Gilbert CM. J Am Chem Soc 1985;57:166–70.
[19] Klingler RJ, Kochi JK. J Phys Chem 1981;85:1731.
[20] Williams DH, Fleming I. Spectroscopic methods in organic chemistry. London: McGraw-Hill Publishing Company Limited; 1966.
[21] Bellamy LJ. The infrared spectra of complex molecules. London: Methuen; 1962.
[22] Tezcan H, Uzluk E. Dyes Pigments 2008;76:733–40.